Rev. Adv. Mater. Sci. 47 (2016) 59-65

SIMULATION OF SMALL-ANGLE X-RAY SCATTERING CURVES TO DETERMINE THE SIZE, SHAPE AND DISTRIBUTION OF SECONDARY PHASES IN DYNAMICALLY AGED ALUMINUM ALLOY 6201

V.D. Sitdikov[1,2], P.S. Chizhov[3], M.Yu. Murashkin[1,2] and R.Z. Valiev[1,2]

[1]Institute of Physics of Advanced Materials, Ufa State Aviation Technical University, Ufa, 450000, Russia
[2]Laboratory for Mechanics of Bulk Nanomaterials, Saint Petersburg State University, Saint Petersburg 98504, Russia
[3]Faculty of Chemistry, Moscow State University, Moscow, 119991, Russia

Received: April 25, 2016

Abstract. In this paper computer simulation of small-angle X-ray scattering (SAXS) curves was applied to determine the size, shape, and distribution of secondary phases formed in the aluminum matrix during dynamic ageing. SAXS patterns were registered in transmission mode for Al-Mg-Si alloys foils. For the first time the spatial distribution of dispersed phase particles was accounted during the simulation of scattering curves. Scattering curves were simulated in the large angular range to improve the accuracy of the results. The method of SAXS was preliminarily tested on similar samples after artificial ageing to validate the used approach.

1. INTRODUCTION

The techniques of small-angle X-ray scattering (SAXS) and small-angle neutron scattering (SANS) are widely used in the study of ageing processes in metallic materials and alloys [1-4]. During a SANS experiment a considerably large sample volume is analyzed due to a relatively weak interaction of neutrons with the material. In SAXS, due to the limited penetration depth of characteristic X-rays into the sample, thin foils or thin surface layers are used for the study. Either for SAXS or SANS the experimental data is the dependence of intensity $I(2\theta)$ of diffracted X-ray quanta (neutrons) on the scattering angle 2θ (the so-called scattering curve).

The analysis of scattering curves in different approaches allows for establishing the processes that take place in the systems with chaotic or partially ordered inhomogeneities.

Earlier models to analyze the scattering curves obtained from powders, films, solutions and also metallic materials were based mainly on the Guinier approach [3]. It being understood that the intensity of registered X-ray quanta $I(q)$ on scattering vector magnitude $q = 4\pi\sin\theta/\lambda$ decreases exponentially with the increase of the scattering angle. The linear part of $\ln I(q)$ dependence on q^2 was used to calculate the electron radius of gyration R_g that is associated with the characteristic dimensions of simple shape homogeneous solids. Mentioned approach allows the determining of the size of the spherical particles during the study of the zone stage of decomposition in the alloys Al-Zn and Al-Ag [3]. However, the drawbacks of the Guinier approach include the limited study area ($q\,R_g < 1.0$) and impossibility to account for the effects of interparticle interference.

The development of SANS/SAXS method with accounting for the structure factor *S(q)* and shape

Corresponding author: V.D. Sitdikov, e-mail: svil@ugatu.su

factor *F(q)* (e.g. with its expansion to spherical harmonics) allows to establish the size and distribution of secondary phases with spherical, cylindrical and core-shell shapes in the materials [2]. Particularly, in [5,6] SANS was applied to the case of artificial ageing T6 (the samples were aged at 170 °C during 24 h) of the aluminum alloys. The results demonstrated the formation of needle-shaped β" – Mg_5Si_6 phase (monoclinic lattice C2/m, *a* = 15.34 Å, *b* = 4.50 Å, *c* = 6.83 Å, β = 106°) particles with a mean diameter of 3.4 ± 0.3 nm and a length of 20±9 [5]. In [6] the formation of needle-shaped particles in the alloy Al-Mg-Si with a diameter of 2.5 nm and a length of 8 nm during artificial ageing T6 was revealed.

On the other hand, in [7] the diameter of secondary phases in the aluminum alloy Al-Mg-Si, as determined by SAXS using Kratky-Porod approach, was 3.6 nm and their length was 16 nm. Meanwhile, transmission electron microscopy (TEM) studies showed that artificial ageing results to the formation of needle-shaped β" particles with a diameter of 2-4 nm and a length of 30-40 nm [6-8]. Thus, in [5,6,7] the calculation of particle diameter by SAXS/SANS correlates well with the TEM studies, whilst the length of the particles is underestimated. At the same time, in this paper the simulation of scattering curves using a modified approach with accounting for the spatial distribution of secondary phases and analysis of sufficient variations of scattering angles allow allowed establishing the TEM-consistent size and shape of secondary phases, as well as determining their spatial distribution.

Unlike artificial ageing, the process of dynamic strain ageing (DSA) may be realized in the alloys as a result of high pressure torsion (HPT) in conditions of large applied strains [10,11]. The process of DSA in the billets is much faster (within several minutes) and progresses at lower temperatures in comparison with the conventional methods of heat treatment or deformation [10,11]. In particular, DSA, when realized by HPT at 130 °C, increases the strength to 412 MPa and electrical conductivity to 55.6% on the International Annealed Copper Standard (IACS) scale [10]. TEM analysis demonstrated that the spherical particles of β-Mg_2Si phase are mostly formed as a result of DSA in contrast to artificial ageing [10-12]. Taking into account the aforementioned data, the influence of size, shape and distribution of secondary-phase particles on the strength and electrical conductivity of aluminum alloys is a highly topical problem.

Resuming, the aim of this work was the application of the modified SAXS approach to determine the size, shape and distribution of secondary phases during dynamic aging of the Al alloy 6201. The modified SAXS approach was previously tested on the samples after artificial aging to compare the results with the well-known literature data.

2. MATERIAL AND METHODS

A series of experiments to study artificial ageing by use of T6 treatment and dynamic ageing were done on the 6201 aluminum alloy with the following main alloying elements concentrations (wt.%): Al-98.0, Mg - 0.81, Si - 0.79, Fe not more than 0.5. The initial aluminum alloy was subjected to HPT for the formation of ultarine-grained structure and DSA. During HPT, the sample between two dies was exposed by 6 GPa pressure with consequent 20 rotations of upper anvil with 1 min^{-1} rotation speed. HPT processing was performed at 130 °C, 180 °C, 200 °C, and 230 °C as active dynamic ageing is observed in the indicated temperature range according to TEM analysis [10].

Rigaku Ultima IV diffractometer with a small-angle attachment was used to record SAXS patterns. Analysis was carried out using a parallel beam of the Cu K_α X-ray obtained in the "Cross Beam Optics" device with the usage of a parabolic multilayer mirror (divergence angle ~ 0.04°), Soller slit 5.0° and thin film collimator with angular divergence of 0.5° on the primary and secondary beams, correspondingly. The thickness of analyzed foils was 80 μm. Scattering by air fluctuations was minimized by evacuating the optical path between the sample and the detector. Measurements were carried out in the interval of angles 2θ from 0.08° to 8.0° with 0.002 step and exposure time of 5 seconds for each step. The average size of the irradiated area was *ca.* 4 mm.

Microstructure of aluminum alloys after artificial and dynamic ageing was also characterized by TEM using the transmission electron microscope JEM 2100 operated at a voltage of 200 kV. TEM samples were prepared by jet polishing in a solution of 20% nitric acid and 80% methanol at -30 °C. TEM micrographs were observed on an area located at the center of the disc-shaped sample's radius.

3. SIMULATION OF SCATTERING CURVES

In the Guinier approach [3] a small-angle scattering curve for spherically symmetric particles is approximated by the expression

$$I(q) = I(0)\exp\left(-q^2R_g^2/3\right), \quad (1)$$

where $I(0)$ is intensity of X-ray quanta at $2\theta = 0°$. For highly elongated particles, the expression (1) transforms to:

$$I(q) = I(0)\exp\left(-q^2 R_g^2 / 2\right), \quad (2)$$

Expressions (1) and (2) allow to calculate the radius of gyration of spherical and cylindrical particles by the formulas, correspondingly:

$$R_g = \frac{\sqrt{3\cdot\left(\ln I(0) - \ln I(q)\right)}}{2}, \quad (3a)$$

$$R_g = \frac{\sqrt{2\cdot\left(\ln I(0) - \ln I(q)\right)}}{2}. \quad (3b)$$

In contrast to the Guinier approach, where the electron radius of gyration R_g is determined by a slope of a scattering curve ($\ln I(q)$ dependence on q^2), in this work the analysis of scattering curves obtained by SAXS was carried out with the use of a modified approach In this approach the dependence of true intensity (the intensity difference between the experimental $I_{sample}(q)$ and background radiation $I_{background}(q)$) was determined as

$$I(q) = I_{sample}(q) - I_{background}(q) = \left|F(q)\right|^2 S(q), \quad (4)$$

where the form factor value *F(q)* stands for the shape (in this work a sphere and a cylinder were considered) and size of particles, and *S(q)* – the so-called structure factor responsible for the interparticle interference. Whilst, the shape factor was defined as the integral over the volume of particles of the dispersed phase *V:*

$$F(\mathbf{q}) = \int_V \Delta\rho(\mathbf{r}) e^{iqr}\, \mathrm{d}r, \quad (5)$$

where $\Delta\rho(\mathbf{r})$ is the contrast (the difference between the mean values of electron density for the dispersion medium and dispersed phase), **r** is the radius vector. The cumulative average of $F(\mathbf{q})$ over angle coordinates gives the scalar-dependent $F(q)$.

In case of spherical particles with the radius R, a well-known expression for shape-factor of homogeneous spherical particle was applied [2]:

$$F^{sphere}(q) = \Delta\rho\int_0^{2\pi}\mathrm{d}\varphi\int_0^{\pi}\mathrm{d}\theta\int_0^{R} e^{iqr\cos\theta} r^2 \sin\theta\,\mathrm{d}r = \Delta\rho\frac{4\pi}{q^3}\left(\sin(qR) - qR\cos(qR)\right). \quad (6)$$

In case of cylinder-shaped particles with the radius R and the length l, the shape-factor was defined as [2]:

$$F^{cylinder}(q,\varphi) = \Delta\rho 4\pi R^3 \times \frac{\sin(qaR\cos\varphi) J_1 qR\sin\varphi}{(qR)^2\sin\varphi\cos\varphi}. \quad (7)$$

Here, $a = l/R$, J_1 is the spherical Bessel function of first order, φ is the angle between the cylinder axis and the scattering vector $\boldsymbol{q}$. The orientation distribution of cylindrical particles was considered as uniform and the scattering factor applied was cumulative average over φ for the function (7).

To account for the interparticle interference the following function was applied [NANO-Solver Software, Ver. 3.7]:

$$S(\mathbf{q}) = 1 + \int_V \left(n(\mathbf{r}) - n_0\right) e^{iqr}\,\mathrm{d}\mathbf{r}, \quad (8)$$

where $n(\mathbf{r})$ is the particle count density function (for the case of equivalent particles

$$n(\mathbf{r}) = n_i(\mathbf{r}) = \sum_{j\neq i}\delta\left(\mathbf{r} - \left(\mathbf{R}_i - \mathbf{R}_j\right)\right),$$

$n_0 = N/V$ is the effective density of N particles in the irradiated volume V. The integral in (8) (taken over the entire irradiated volume of the sample V) is a so-called «particle packing fraction». Here, if the structure factor in Eq. (4) is equal to one (packing fraction equals to zero), then the particles in the medium are distributed randomly. In case of non-random location of the particles (interparticle correlations exist), the certain $S(\mathbf{q})$ dependence appears. Simulation was carried out using a simple model of constant mean distances between the particles that varies during the least-squares refinement.

The (q) dependence was obtained experimentally by analysing the scattering curve in the absence of the sample. When simulating the experimental scattering curve (q), the results of calculation by equation (4) were also convolved with the instrumental function calculated with consideration of the size of the X-ray tube focus, the distance between the focal spot, the test sample and the detector, slits aberration, the angular divergence of the primary and secondary beams, the sizes of target area [NANO-Solver Software, Ver. 3.7]. In contrast to traditional SAXS/SANS methods when the analysis are conducted in the range of angles 2θ from 0.1° to 1.5°, in this work the data were recorded up to 8° to increase the accuracy of the data.

4. RESULTS AND DISCUSSION

The results of TEM analysis demonstrated that needle-shaped secondary phases Mg_5Si_6 (Fig. 1)

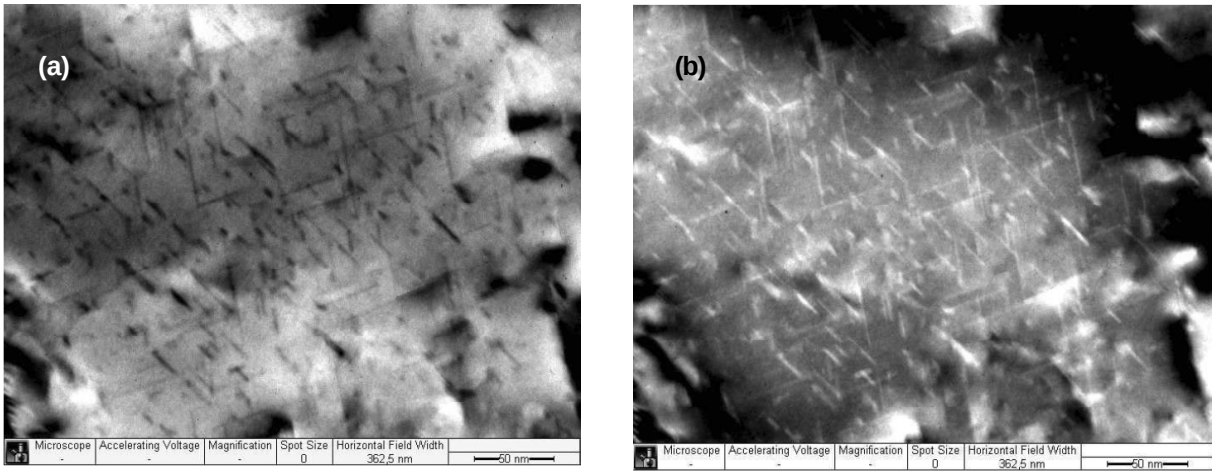

Fig. 1. Bright-field (a) and dark-field (b) TEM images of aluminum alloy 6201 after T6 treatment.

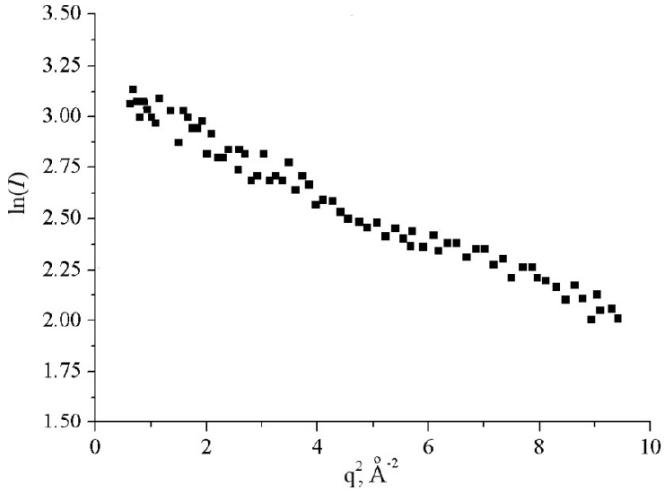

Fig. 2. SAXS curve for Al alloy 6201 after artificial T6 ageing.

are formed in the microstructure of aluminum alloy 6201 subjected to artificial (T6) ageing. At the same time, the processing of TEM patterns showed that the mean radius of particles was about 3 nm and the length was about 30 nm. TEM analysis carried out elsewhere also reveal the fact that needle-shaped Mg_5Si_6 particles of a diameter 2-4 nm and a length of 30-40 nm are formed in the aluminum alloy Al-Mg-Si after conventional ageing of T6 treatment [8,9].

Let's first consider the analysis of the shape and size of secondary phase particles in the Guinier approach and then in a modified one. Fig. 2 shows the linear part of the scattering curve in the coordinates $\ln(I)$-q^2 for aluminum alloy 6201 after artificial T6 ageing. Calculation of R_g according to formula (3b) gives the mean radius of highly elongated particles of ~ 5 nm. This value slightly differs from the results obtained from the analysis of TEM images. The former case is apparently due to certain restrictions of the Guinier approach. Detailed analysis of the scattering curves in a modified approach was carried out in a fairly large range of 2θ angle variations.

Fig. 3 shows the scattering curves for aluminum alloy 6201 at artificial T6 ageing and dynamic ageing after HPT at a variety of temperatures. Characteristic feature of such curves is a point of inflexion at an angle of 2θ less than 0.2°. As shown in the figure, these points for the experimental curves $I(2\theta)$ for the samples subjected to DSA are located at smaller angles comparing with the curve for the sample after T6 treatment. This fact indicates that the strengthening secondary phases are of higher size in case of DSA than that for T6 treatment. Scattering curves were simulated in aforementioned approach to determine the size, shape and distribution of secondary phases. In Fig. 3 the solid lines resulted from simulation of experimental scattering curves. As is can be seen, the experimental curves are described well in all of the cases (weighted $(1/\sigma^2)$ *R*-factor in all cases less than 1%).

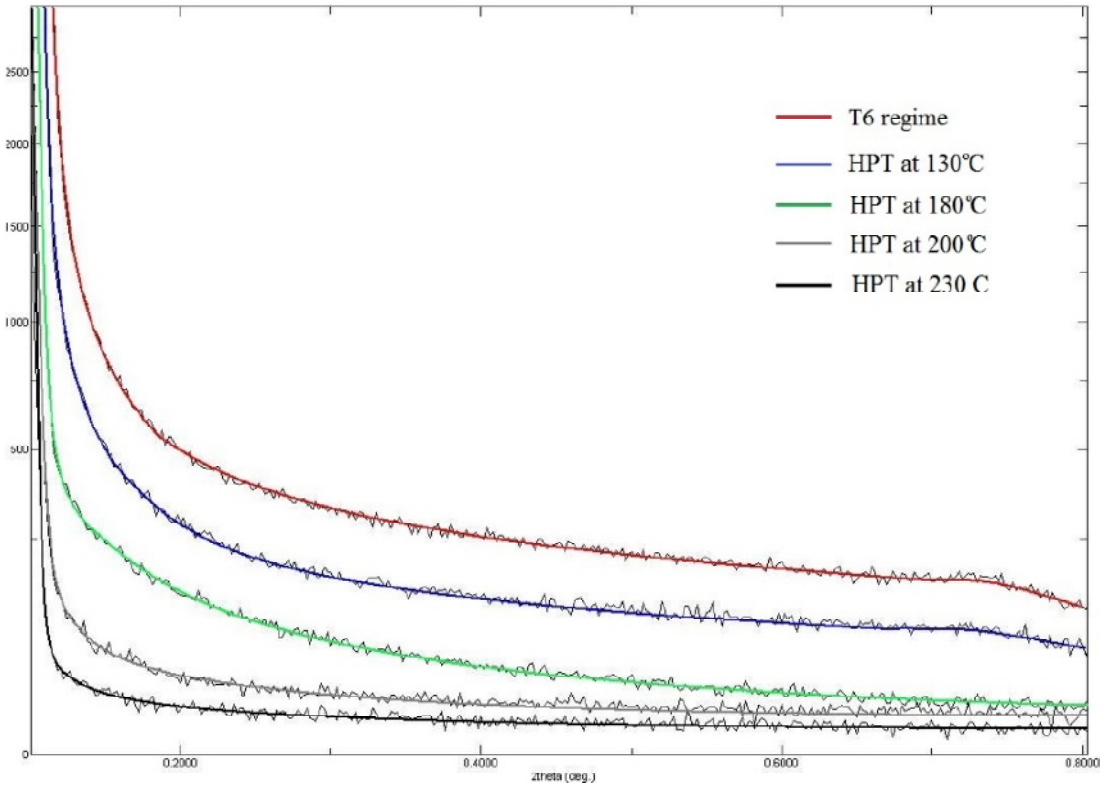

Fig. 3. Experimental and simulated scattering curves of Al alloy 6201 after different treatment.

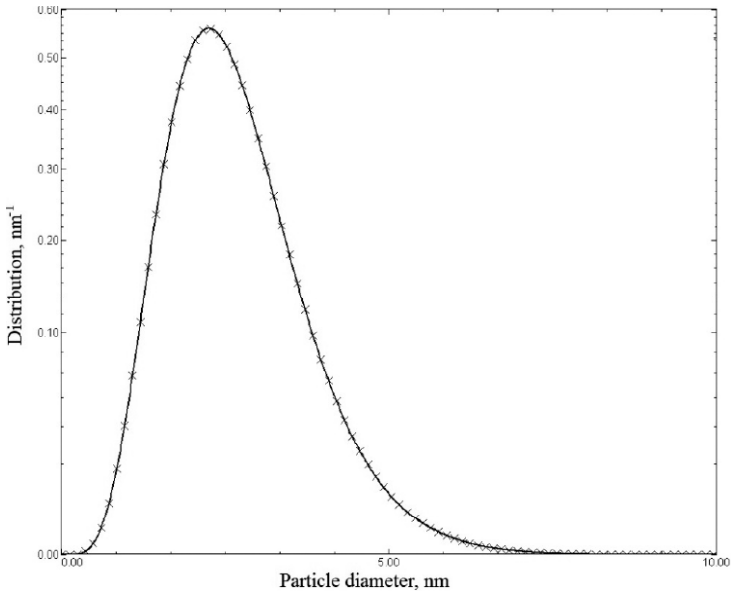

Fig. 4. Size distribution of secondary-phase particles. Aluminum alloy 6201 after T6 treatment.

Fig. 4 shows the results of particle-size distribution for T6 treatment when a cylindrical shape (with constant *a*) was used for the simulation. A mean particle diameter in a modified approach was d = 2.4 nm and a mean particle length was *ca.* 35 nm. As was shown above, TEM data give a mean particle radius of about 3 nm and particle length about 30 nm. Thus, the application of a modified approach to the analysis of a scattering curve leads to sufficiently good prediction of the size and shape of secondary-phase particles. The results of scattering curves analysis in a modified approach also correlates well with that obtained by SAXS/SANS methods in the works [5,6,7]. In these studies, the particle diameter is in good agreement with the TEM results and the length of particles is underestimated. Whilst, in this study the analysis of a scattering curve in a wide angular range leads

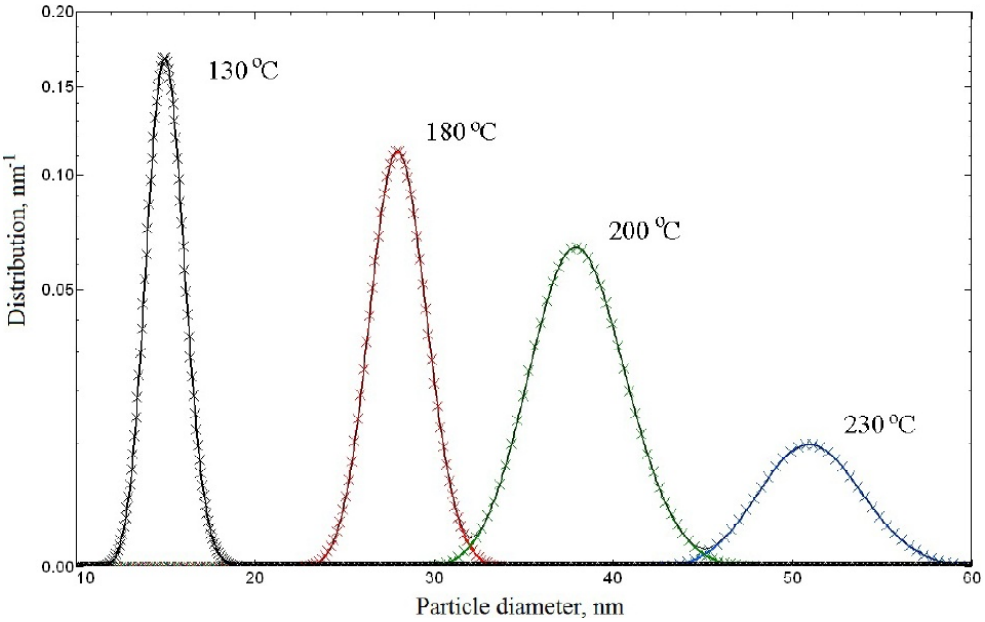

Fig. 5. Size distribution of spherical secondary-phase particles in aluminum alloy 6201 resulted from DSA at various temperatures.

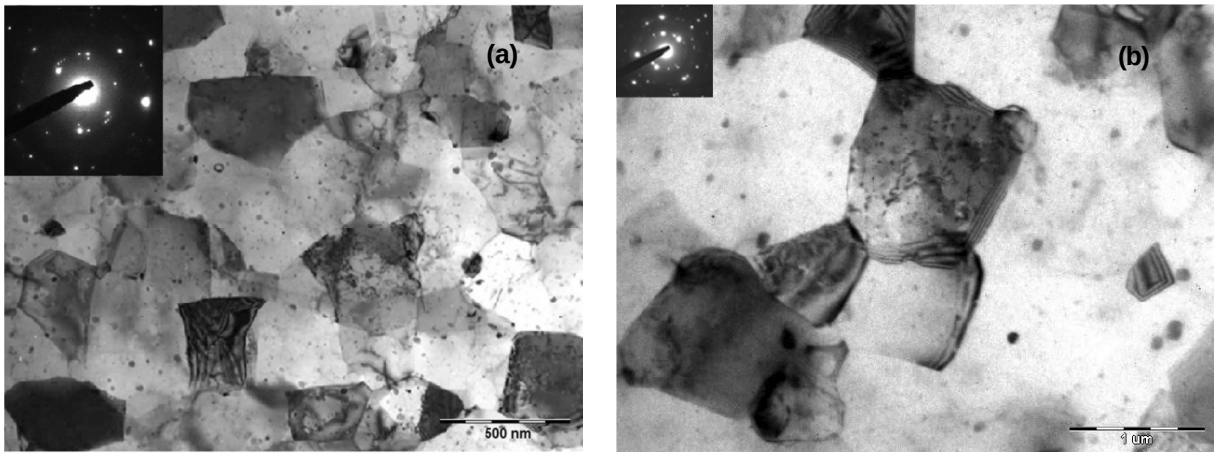

Fig. 6. The images of microstructure of alloy 6201 illustrating the presence of Mg_2Si-phase particles in the aluminum matrix at various temperatures: (a) - 130 °C, (b) - 200 °C.

to a good correlation of a particle and length diameter with the TEM results.

Application of this approach to DSA also allows to establish the size, shape and distribution of the secondary phases. The calculated secondary phase particles size distributions for different treatment regime are shown in Fig. 5. As is seen in the figure, the DSA process that was carried out at a temperature of 130 °C results to the formation of spherically-shaped secondary phase particles with a diameter of 15 ± 4 nm (Table 1). Increase of the DSA temperature from 130 °C to 230 °C leads to pronounced changes in the structure. While the shape of particles remains spherical, a mean particle size increases to 51 ± 7 nm (Table 1). Whilst, the degree of particle dispersion also increases (Fig. 5). The obtained values correlate well with the TEM results (Fig. 6). TEM images give the possibility to identify the spherically-shaped Mg_2Si particles at grain boundaries as well as inside the grain. Calculations of TEM images show that a mean size of particles at 130 °C was 10 nm, at 180 °C - 30 nm, at 200 °C and 230 °C - 38 nm and 51 nm, correspondingly (Table 1). The obtained values correlate well with the results of SAXS studies (see Fig. 5).

5. CONCLUSIONS

Simulation of SAXS curves in a modified approach allows to define the shape, size and distribution of

Table 1. Microstructure parameters obtained by SAXS and TEM (d_n is the diameter of needles, l is the length of needles, d_s is the diameter of spheres).

Treatment	SAXS	TEM	
	Form and size of precipitates, nm	Grain size, μm	Form and size of precipitates, nm
T6	Needles (d_n/l) 2.4/35	62	Needles (d_n/l) 3.0/30
HPT at 130 °C	Spheres (d_s) 15	0.27	Spheres (d_s) 10
HPT at 180 °C	Spheres (d_s) 27	0.45	Spheres (d_s) 30
HPT at 200 °C	Spheres (d_s) 37	0.72	Spheres (d_s) 38
HPT at 230 °C	Spheres (d_s) 52	0.95	Spheres (d_s) 51

secondary-phase particles during artificial and dynamic ageing. It was revealed, that during artificial ageing cylindrically-shaped Mg_2Si secondary phases with a diameter of 2.4 nm and a length of 35 nm are formed in the alloy. During DSA spherically-shaped Mg_5Si_6 secondary particles are formed. The increasing of the temperature during the DSA procedure from 130 °C to 230 °C leads to an increase in the secondary-phase particle diameter from 15 nm to 51 nm, with the corresponding purification of the aluminum matrix. At the same time, the obtained results are of much importance to assess the contribution of the dispersion hardening.

ACKNOWLEDGMENTS

This work was supported by the Russian Federal Ministry for Education and Science (through RZV Grant No. 14.B25.31.0017). V.D. Sitdikov gratefully acknowledges the financial support of this study from the Ministry of Education and Science of Russia (governmental task № 11.729.2014K).

REFERENCES

[1] O. Glatter and O. Kratky, *Small-Angle X-ray Scattering* (Acad. Press Inc. Ltd, London, 1982).

[2] D.I. Svergun and L.A. Feygin, *X-ray and neutron low-angle scattering* (Nauka, Moscow, 1986), In Russian.

[3] A. Guinier and G. Fournet, *Small-angle scattering of X-rays* (Wiley, New York, 1955).

[4] F. De Geuser and A. Deschamps // *Comptes Rendus Physique* **13** (2012) 246.

[5] P. Donnadieu, E Carsughi, A. Redja'imia, C. Diot and G. Lapasset // J. Appl. Cryst. **31** (1998) 212.

[6] D. Bardel, M. Perez, D. Nelias, A. Deschamps, C.R. Hutchinson, D. Maisonnette, T. Chaise, J. Garnier and F. Bourlier // *Acta Mater*. **62** (2014) 129.

[7] C.-S. Tsao, C.-Y. Chen, U-S. Jeng and T.-Y. Kuo // *Acta Mater*. **54** (2006) 4621.

[8] H.J. Roven, M. Liu and J.C. Werenskiold // *Mater. Sci. Eng. A* **483-484** (2008) 54.

[9] L. Cui, Z. Liu, X. Zhao, J. Tang, K. Liu, X. Liu and C. Qian // *Trans. Nonferrous Met. Soc. China* **24** (2014) 2266.

[10] R.Z. Valiev, M.Yu. Murashkin and I. Sabirov // Scripta Mater. **76** (2014) 13.

[11] I. Sabirov, M.Yu. Murashkin and R.Z. Valiev // *Mater. Sci. Eng. A* **560** (2013) 1.

[12] V.D. Sitdikov, P.S. Chizhov, M.Yu. Murashkin, A.A. Goidenko and R.Z. Valiev // *Mater. Char.* **110** (2015) 222.